

High resolution measurements of the switching current in a Josephson tunnel junction: Thermal activation and macroscopic quantum tunneling

A. Wallraff,* A. Lukashenko,[†] C. Coqui, T. Duty,[‡] and A. V. Ustinov
Physikalisches Institut III, Universität Erlangen-Nürnberg, D-91058 Erlangen, Germany
(Dated: November 5, 2018)

We have developed a scheme for a high resolution measurement of the switching current distribution of a current biased Josephson tunnel junction using a timing technique. The measurement setup is implemented such that the digital control and read-out electronics are optically decoupled from the analog bias electronics attached to the sample. We have successfully used this technique to measure the thermal activation and the macroscopic quantum tunneling of the phase in a small Josephson tunnel junction with a high experimental resolution. This technique may be employed to characterize current-biased Josephson tunnel junctions for applications in quantum information processing.

I. INTRODUCTION

The current-biased Josephson tunnel junction is an ideal system to study both thermal activation^{1,2} and quantum tunneling^{3,4} in a controllable experimental environment. The dynamics of such a junction is equivalent to that of a particle in a tilted washboard potential^{5,6}. The process of the particle escape from a metastable state in this system can be characterized, by analyzing the transition of the particle from a state in which it is localized in a potential well to a state in which it runs down the potential. This corresponds to the transition of the Josephson junction from the superconducting zero-voltage state to a finite voltage state in the presence of an applied bias current. At high temperatures the escape is dominated by thermal activation across the barrier, at low temperatures it is determined by quantum tunneling through the barrier. The rate with which the particle escapes from the well depends on the detailed shape of the potential, the dissipation in the system and the temperature of the thermal bath to which the system is coupled.

Thermal activation in a current biased Josephson junction has been studied both theoretically and experimentally for large damping^{7,8}, intermediate to low damping^{9,10,11} and extremely low damping^{11,12}. At low temperatures the quantum mechanical properties of Josephson junctions have been investigated in relation to macroscopic quantum tunneling (MQT)^{13,14,15}, energy level quantization (ELQ)^{12,16} and macroscopic quantum coherence (MQC)¹⁷. Recently, the quantum mechanical properties of Josephson junction systems have regained interest in the view of their possible application for solid state based quantum information processing^{18,19,20}. The prospects of superconducting devices containing Josephson junctions for use as carriers of quantum information has been strengthened by recent encouraging experimental results^{21,22,23}.

In this paper we present a measurement technique implemented for the characterization of the quantum properties of current biased phase qubits. The measurement scheme is based on a high resolution measurement of the junctions switching current⁹ using a timing technique.

The measurement setup was tested by performing measurements of both thermal activation and quantum tunneling in a current biased small Josephson junction.

In Sec. II, the Stewart-McCumber model describing the dynamics of the phase in a Josephson junction is briefly reviewed in relation to thermal activation and quantum tunneling of the phase. The measurement technique and the setup implemented for its realization is described in Sec. III. The switching current distributions obtained over a large range of temperatures are presented in Sec. IV. The relative resolution of these measurements is compared with other results from literature in Sec. V. In Sec. VI, the data in the thermal regime is analyzed in the view of the low dissipation in the junction. The crossover temperature to the quantum regime is determined and the measured switching current distributions are compared to the quantum predictions. Finally the results are summarized in Sec. VII.

II. MODEL

In the Stewart-McCumber model^{5,6}, the dynamics of a current biased Josephson tunnel junction is described by an equation of motion for the phase difference ϕ

$$C \left(\frac{\Phi_0}{2\pi} \right)^2 \ddot{\phi} + \frac{1}{R} \left(\frac{\Phi_0}{2\pi} \right)^2 \dot{\phi} + I_c \frac{\Phi_0}{2\pi} \sin(\phi) - I \frac{\Phi_0}{2\pi} = 0, \quad (1)$$

where Φ_0 is the magnetic flux quantum, C is the capacitance, R the effective junction resistance and I_c the fluctuation free critical current of the junction, see Fig. 1a. Here, I is the externally applied bias current. The equation of motion (1) is equivalent to the damped motion of a particle of mass $m_\phi = C(\Phi_0/2\pi)^2$ in an external potential $U^\phi(\phi)$ along the generalized coordinate ϕ

$$m_\phi \ddot{\phi} + m_\phi \frac{1}{RC} \dot{\phi} + \frac{\partial U^\phi(\phi)}{\partial \phi} = 0. \quad (2)$$

In Eq. (2) the damping coefficient is $1/RC$ and the potential is given by

$$U^\phi(\phi) = E_J (-\gamma\phi - \cos\phi), \quad (3)$$

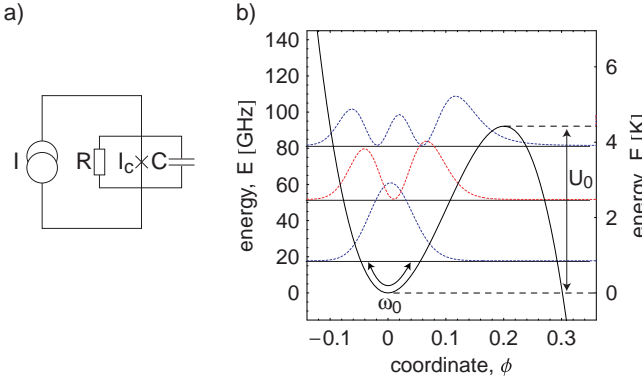


FIG. 1: a) Resistively, capacitively shunted junction (RCSJ) model. b) U^ϕ versus ϕ calculated for a junction with the parameters as used in experiments and biased at $\gamma = 0.995$. The barrier height U_0^ϕ and the oscillation frequency ω_0^ϕ are indicated. Numerically calculated energy levels and the squared wave functions are shown.

where $E_J = \Phi_0 I_c / 2\pi$ is the Josephson coupling energy and $\gamma = I/I_c$ is the normalized bias current. $U^\phi(\phi)$ is a sinusoidal potential (3) with an amplitude proportional to E_J , which is tilted proportionally to the applied bias current γ . Because of these properties $U^\phi(\phi)$ is called often washboard potential.

In the absence of thermal and quantum fluctuation and for bias currents $\gamma < 1$, the junction is in the zero voltage state, corresponding to the particle being localized in one of the potential wells (see Fig. 1b). At finite temperatures $T > 0$, the particle may escape from the well at bias currents $\gamma < 1$ by thermally activated processes^{7,9,10,24,25,26} and also by quantum tunneling through the barrier^{12,13,14,15,27}. The rate at which both processes occur depends on the barrier height

$$U_0^\phi = 2E_J \left[\sqrt{1 - \gamma^2} - \gamma \arccos(\gamma) \right], \quad (4)$$

the oscillation frequency of the particle at the bottom of the well

$$\omega_0^\phi = \sqrt{U''^\phi/m_\phi} = \omega_p (1 - \gamma^2)^{1/4}, \quad (5)$$

and the damping in the junction. Here $\omega_p = \sqrt{2\pi I_c / \Phi_0 C}$ is the plasma frequency. For $\gamma \rightarrow 1$, Eq. (5) can be approximated as

$$U_0^\phi \approx E_J \frac{4\sqrt{2}}{3} (1 - \gamma)^{3/2}. \quad (6)$$

At high temperatures the escape of the particle from the well is dominated by thermally activated processes, which occur with a bias-current dependent rate of^{1,2}

$$\Gamma_t = a_t \frac{\omega_0^\phi}{2\pi} \exp \left(-\frac{U_0^\phi}{k_B T} \right). \quad (7)$$

Here a_t is a temperature and damping dependent thermal prefactor.

As the temperature T is lowered, the thermal activation is exponentially suppressed. At temperatures below the so called cross-over temperature T^* the quantum tunneling rate of the particle through the barrier exceeds the thermal activation rate²⁸. The tunneling rate of the phase is calculated in the Wentzel-Kramers-Brillouin (WKB) approximation for a particle of mass m^ϕ tunneling through the potential barrier described by U^ϕ . The effect of damping with the characteristic coefficient $a = 1/(2RC\omega_0^\phi) = 1/(2Q)$, where $Q = \omega_0^\phi RC$ is the junction quality factor, is considered in terms of a coupling to a bath of harmonic oscillators^{3,29,30}. The rate is then given by

$$\Gamma_q = A \exp(-B) \quad (8)$$

with

$$A = \sqrt{60} \omega_0^\phi \left(\frac{B}{2\pi} \right)^{1/2} (1 + \mathcal{O}(a)), \quad (9)$$

$$B = \frac{36U_0^\phi}{5\hbar\omega_0^\phi} (1 + 1.74a + \mathcal{O}(a^2)). \quad (10)$$

As in Eq. (7), the values of Γ_q , U_0^ϕ , and ω_0^ϕ depend on I .

At low temperature and small damping the energy of the small oscillations of the phase at the bottom of the well is quantized, see Fig. 1b. The energy level quantization has been observed experimentally both below¹² and above T^* ^{16,31}. The escape of the phase from the well in the presence of quantized energy levels was discussed theoretically by Larkin and Ovchinnikov in Ref. 32. This theory allows for the calculation of the bias current dependent escape rate $\Gamma(I)$ considering the escape of the particle from the well by tunneling from any energy level. The occupation of the levels can be calculated for finite temperatures and in the presence of microwaves using a master equation approach. Previous measurements of energy level quantization have been compared with the predictions of this theory and good agreement was found^{33,34}. This theory has also been used to explain switching current distributions for non-stationary distributions of the phase at high current ramp rates and above the cross-over temperature³¹. Here, we analyze our data for the escape of the phase in the presence of energy levels with a separation comparable to the bath temperature $k_B T$ at temperatures above T^* in the framework of this theory.

III. MEASUREMENT TECHNIQUE AND SETUP

The escape of the phase in a Josephson tunnel junction is experimentally investigated by performing a statistical measurement of the current at which the junction switches from the zero-voltage state to a finite voltage state⁹. There are two different well established methods to perform such a measurement. One method con-

sists of applying a fixed bias current $I < I_c$ to the junction and measuring the time between the application of the current and the appearance of a voltage across the junction^{17,35}. This corresponds to a direct measurement of the lifetime $\tau(I)$ of the particle in the well. The inverse of the lifetime corresponds to the escape rate $\Gamma(I)$. In the other method, the bias current applied to the junction is ramped up at a constant rate \dot{I} and the current I at which the junction switches from the zero-voltage to a finite voltage state is recorded⁹. The switching current probability distribution $P(I)$ is found by accumulating a large number of switching currents I and generating a histogram. From the $P(I)$ distribution the bias current dependent escape rate

$$\Gamma(I) = \dot{I} \ln \frac{\int_I^\infty P(I') dI'}{\int_{I+\Delta I}^\infty P(I') dI'}. \quad (11)$$

can be reconstructed⁹ and compared with the theoretical predictions.

A. Experimental setup

In order to measure the switching current distribution of a Josephson tunnel junction with a high accuracy, we have developed a measurement setup in which the analog biasing electronics and the sample are electrically isolated from the digital control electronics using an optical fiber link. Using a universal time interval counter with 20 GHz time-base, the switching current is determined by measuring the time between the zero crossing of the bias current ramped up at a constant rate and the switching of the junction to the finite voltage state.

In the following the elements of the experimental setup are discussed starting from the sample cell mounted at the cold finger of the dilution refrigerator, the cold and warm filters in the dc-bias lines, the room temperature analog electronics, the optical fiber link and finally the digital control and data acquisition electronics, see Fig. 2.

1. Sample Cell and Wiring

The sample, typically fabricated on a 5×5 mm² chip, is mounted in a closed rf-tight copper cell to shield it from electromagnetic radiation from the environment. The sample cell is thermally anchored to the cold finger of a dilution refrigerator. For current-biasing the Josephson junction and measuring the voltage across it, four wires are fed through microwave filters into the cell. Inside the cell the wires are thermally anchored and connected via wire bonds to the sample. Each microwave filter consists of a commercially available⁴⁵ 1 meter piece of a 0.5 mm in diameter, lossy stainless steel coaxial line with a $50 \Omega/m$ inner conductor made from Ni/Cr (80%/20%) which is soldered into the wall of the cell. This type of filter, also called thermocoax filter³⁶, has an attenuation

of more than 50 dB/m at frequencies above 1 GHz. Alternatively, we have also used copper powder microwave filters¹², consisting of a few meters of resistive wire coiled up in a 10 cm long copper tube filled with 10 μm grain-size copper powder and mounted in the wall of the cell. If heating of the sample at large bias currents is an issue, the total dc resistance of this filter may easily be adjusted by choosing a different wire material and diameter. This type of filter is designed to have an attenuation of more than 50 dB per piece above 1 GHz. All required additional wires for heaters, temperature sensors, coils etc. were fed into the cell through microwave filters of this type. Another possible type of cryogenic microwave filter, which has not been tested in our setup, is based on a micro-fabricated distributed RLC filter³⁷.

The sample leads are passed to the 1 K stage of the cryostat in a tightly twisted loom of superconducting wire and filtered using a low pass RC filtering stage with a 3 dB cutoff frequency of approximately 50 kHz, which is thermally anchored at the 1 K pot. The wiring is further fed to the top of the cryostat in a loom of twisted copper pairs shielded separately from the sensor and control wiring of the cryostat. At room temperature all wires are going through low pass π -type feedthrough filters with a cutoff frequency of about 10 MHz. After the last filtering stage the wires are separated into shielded pairs which are connected to the analog biasing electronics.

2. Analog Electronics

The sample is current biased by a voltage controlled current source with selectable output-current ranges. The source current I is proportional to the input voltage V_I in the range from -10 V to 10 V. The control voltage V_I is a sawtooth waveform with an adjustable voltage ramp rate generated by charging a capacitor with a constant current. The sawtooth signal is started upon a digital trigger signal at the set input (S). The voltage ramp is stopped by a digital trigger signal at the reset input (R), see Fig. 2.

The current flowing through the sample is monitored by measuring the voltage drop $V_{I,\text{Mon}}$ across the biasing resistor R_I using an instrumentation amplifier. The voltage V across the junction is measured using a fast FET instrumentation amplifier (amplification $\times 1000$). Both voltages $V_{I,\text{Mon}}$ and V are fed to two independent Schmidt triggers with adjustable threshold and window voltages. The current trigger is calibrated to generate a TTL pulse $V_{I,\text{TTL}}$ upon the zero-crossing of the bias current. The voltage trigger is set up to generate a TTL pulse V_{TTL} when the junction switches from the zero voltage to a finite voltage state. The trigger window is adjusted wide enough to avoid voltage noise induced triggering. The voltage trigger signal V_{TTL} is simultaneously used to stop the current ramp. To avoid a ground loop in the signal lines an opto-coupler is used at the reset input of the sawtooth generator.

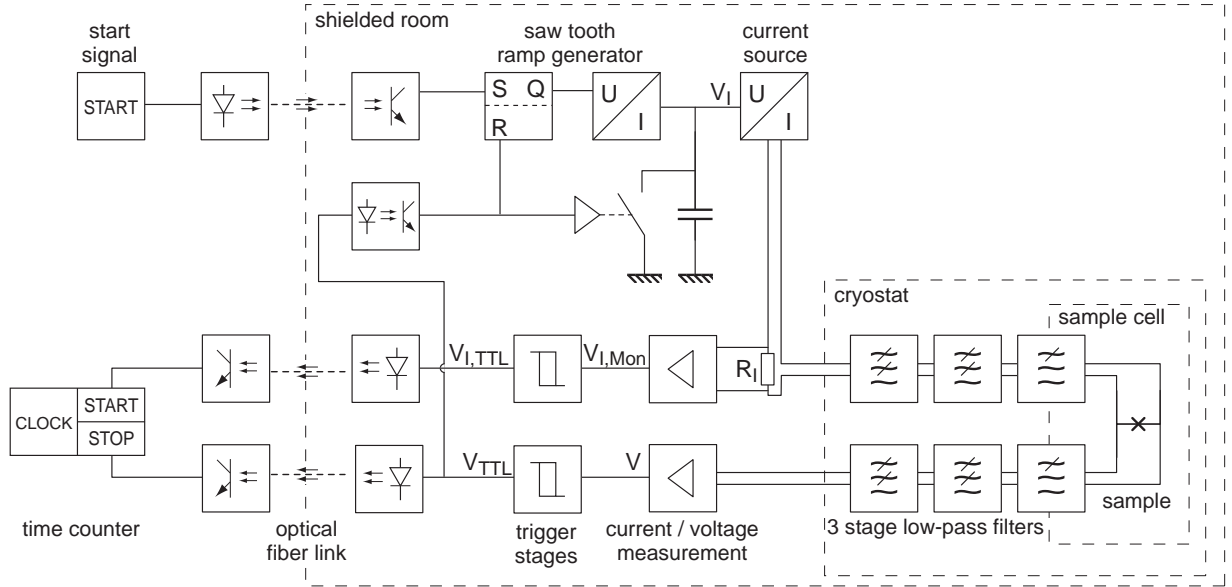


FIG. 2: Schematic of the measurement setup. (A detailed explanation is found in the text.)

All analog electronics components described above have been specifically designed and implemented for these measurements. The supply voltage is delivered by lead accumulators. Care has been taken to avoid ground loops. All electronics is grounded at a single grounding point on the top of the cryostat. The cryostat and the analog electronics are placed inside a stainless steel shielded room. Outside of the shielded room the pumping lines of the cryostat are electrically isolated from the gas handling system and the pumps. The cryostat is connected to the shielded room through the pumping lines.

To perform the current measurement, the current trigger signal $V_{I,TTL}$ and the voltage trigger signal V_{TTL} are converted to digital optical pulses which are passed out of the shielded room via optical fibers. Outside the shielded room both signals are converted back to TTL level electric signals. Conversely, for starting the current ramp a TTL pulse is passed via the optical fiber link into the shielded room. The arrangement of the analog electronics setup is shown in Fig. 2.

3. Digital Control and Data Acquisition Electronics

A square wave generator provides a TTL signal at a rate ν_I which is used to start the current ramp with the same repetition rate ν_I . In each cycle of the measurement the bias current is increased at a fixed rate \dot{I} until the switching current I is reached. The optically decoupled current and voltage trigger signals are then supplied to the start and stop inputs of a universal time interval counter to measure the time τ between the triggers with a resolution of approximately 25 ps. Having calibrated the current ramp rate \dot{I} the switching current can be calculated from the time as $I = \dot{I}\tau$.

Our method has a high instrumental resolution $\Delta I = \dot{I} 25 \text{ ps}$ of the current measurement. For typical ramp rates between 0.1 A/s and 1 A/s as used in the experiments presented here, a relative *instrumental current resolution* between $\Delta I/I = 2.5 \cdot 10^{-12}$ and $25 \cdot 10^{-12}$ can be achieved. This value is much better than that achievable using a 16 bit A/D converter for direct current measurements with $\Delta I/I = 0.15 \cdot 10^{-6}$.

Similar time-based methods for measuring the junctions critical current at a constant current ramp rate^{24,25} or the lifetime of the zero-voltage state of a junction at a constant applied bias current^{17,35} have been implemented by other groups.

The time interval counter⁴⁶ used in our setup allows for “the on-the-fly” generation of switching current histograms from the acquired data during the measurement. This feature is very useful for online monitoring of switching current histograms with changing experimental conditions, e.g. when doing spectroscopic measurements by applying microwave radiation to the sample or when searching for parasitic noise sources.

The temperature controller of the dilution refrigerator is installed inside the shielded room. It can be powered either by two lead accumulators or by an isolation transformer. The electrical ground of the controller is anchored on the cryostat. The temperature controller is computer controlled via an optical fiber link.

IV. EXPERIMENTAL OBSERVATIONS

The experiments were performed using a high quality $5 \times 5 \mu\text{m}^2$ tunnel junction fabricated on an oxidized silicon waver using a standard Nb/Al-AlO_x/Nb trilayer process. The junction had a nominal critical current density of

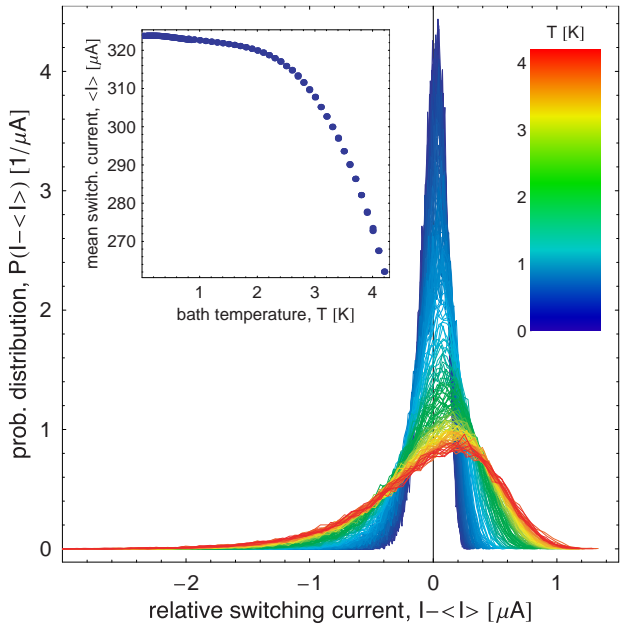


FIG. 3: Switching current distributions $P(I - \langle I \rangle)$ at bath temperatures between $T = 4.2$ K and $T = 25$ mK. The temperature is color coded according to the scale shown in the plot. In the inset the mean value $\langle I \rangle$ of the switching current distribution is plotted versus the bath temperature T .

$j_c \approx 1000$ A/cm², a nominal capacitance of $C \approx 1$ pF and a subgap resistance of $R > 500$ Ω below 1.0 K.

The switching current distribution of the sample was measured at bath temperatures T between 4.2 K and 25 mK. The current was ramped up at a constant rate of $\dot{I} = 0.245$ A/s with a repetition rate of $\nu_I = 500$ Hz. Typically 10^4 switching currents were recorded at each temperature. Histograms of the switching currents were calculated with bin widths of approximately 10 nA in order to determine the $P(I)$ distributions. In Fig. 3 the measured switching current distributions are plotted versus T . To show all histograms in the same plot, the switching probability P has been plotted versus $I - \langle I \rangle$, where $\langle I \rangle$ is the temperature dependent mean value of the switching current shown in the inset of Fig. 3. It is observed that the width of the $P(I)$ distributions decreases with temperature and then saturates at low temperatures, as expected.

The standard deviation σ_I of $P(I)$ is plotted versus T in Fig. 4. In the temperature range between 1 K and approximately 300 mK, σ_I decreases with T , indicating the temperature dependent thermal activation of the phase across the barrier. At the characteristic temperature $T^* \approx 300$ mK, σ_I saturates at approximately 115 nA suggesting that the escape of the phase is dominated by quantum tunneling through the barrier. In Sec. VI, the $P(I)$ distributions in both the thermal and the quantum regime are analyzed quantitatively and compared with existing models.

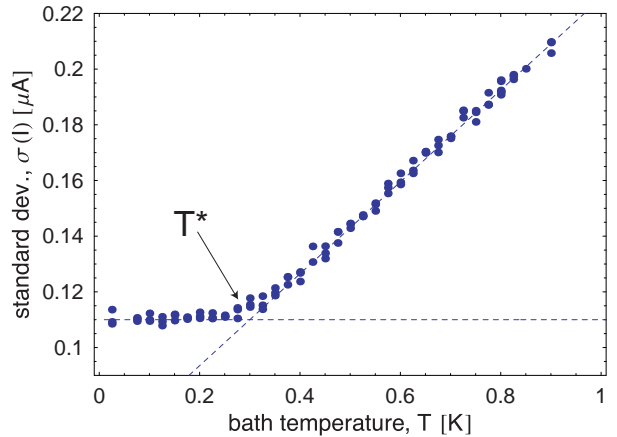


FIG. 4: Standard deviation σ_I of the $P(I)$ distributions versus the bath temperature T . The cross-over temperature T^* is indicated.

V. EXPERIMENTAL RESOLUTION

We have compared the experimental resolution of our switching current measurements performed with the experimental setup described above to the resolution of such measurements presented in literature. Since the limiting resolution of the measurement technique is not always stated in existing publications, we have focused our comparison on the minimum measured width of the switching current distribution mentioned in the articles. To allow for comparison among very widely varying sample parameters, we express the width with respect to the critical current of the measured junction. As a measure of the width we have considered the standard deviation σ_I of the $P(I)$ distributions. If the values of σ_I were not available in the reference, we evaluated the full width at half maximum of $P(I)$. In some of the evaluated references the effect of energy level quantization is investigated. This typically leads to features on the distributions which are more narrow than σ_I . In such cases^{12,16} we have taken the width of these smaller features. If data of multiple samples were discussed in a reference, the data of the sample with the smallest relative $P(I)$ width is considered.

In Tab. I the collected data are summarized. First, we note that our sample has a high critical current and a relatively small capacitance, leading to a comparatively high cross-over temperature. Only in Refs. 15,27 higher cross-over temperatures have been reported. Most of the experiments listed in Tab. I reach measured relative widths σ_I/I_c down to a few 10^{-3} . Only in a few experiments the smallest relative width is a few times 10^{-4} . The measurements we present here show a resolution which is close to the best measurements of this type performed so far, see last row of Tab. I. We stress that we have not performed any digital filtering or data processing neither on the raw data nor on the switching current distributions presented here. In microwave spe-

TABLE I: Experimental resolution in Josephson junction switching current experiments. Listed are the reference from which data has been extracted (col 1), the focus subject of the respective reference (col 2), the critical current I_c of the measured sample (col 3), the standard deviation σ_I of the most narrow measured switching current distribution (col 4), the junction capacitance C (col 5), the effective junction resistance R (col 6), the cross-over temperature T^* (col 7), the junction dimensions (col 8), and the materials used for junction fabrication (col 9).

Refs.	focus	I_c [μA]	σ_I [μA]	σ_I/I_c	C [pF]	R [Ω]	T^* [mK]	dimensions [$\mu\text{m} \times \mu\text{m}$]	material
Washburn <i>et al.</i> ²⁷	MQT	57.4	—	0.9×10^{-3}	0.67	—	500	1.2×0.13	Nb-Nb ₂ O ₅ -Nb
	MQT	57.4	—	1.5×10^{-3}	12.00	—	150	1.2×0.13	Nb-Nb ₂ O ₅ -Nb
Devoret, Martinis <i>et al.</i> ^{12,13}	MQT, ELQ, TA	9.489	—	0.4×10^{-3}	6.35	190	37	10×10	Nb-Nb ₂ O _x -PbIn
Silvestrini <i>et al.</i> ²⁴	TA	162	0.245	1.5×10^{-3}	500	—	—	100×50	Nb-Nb ₂ O _x -Pb
Vion <i>et al.</i> ⁷	TA	0.040	—	0.4×10^{-3}	0.00015	—	—	—	Al-AlO _x -Al
Castellano <i>et al.</i> ¹⁰	TA	160	—	2×10^{-3}	0.8	—	—	4×4	Nb-Al-AlO _x -Nb
Silvestrini <i>et al.</i> ¹⁶	TA	47.0	—	7×10^{-3}	5.5	20×10^3	—	10×10	Nb-Al-AlO _x -Nb
	ELQ	47.0	—	0.7×10^{-3}	5.5	20×10^3	—	10×10	Nb-Al-AlO _x -Nb
Ruggiero <i>et al.</i> ¹¹	TA	175	0.300	2×10^{-3}	2.5	—	—	5×5	Nb-Al-AlO _x -Nb
this work	MQT, TA	315.0	0.115	0.4×10^{-3}	1.00	500	300	5×5	Nb-Al-AlO _x -Nb

troscopy experiments performed on the same sample³⁸ we have observed photon absorption peaks which showed even smaller relative widths than the switching current distributions presented here. In test experiments we have measured current histograms of relative width down to 1.5×10^{-4} , which is the limiting experimental current resolution achievable in our setup at the present time. These tests have been performed with the junction biased in the resistive state but otherwise with experimental conditions identical to those used for performing switching current measurements.

We note that the *instrumental resolution* of the switching current measurements by a timing technique as implemented in this setup is extremely high as in comparison to other approaches using analog to digital converters^{10,12,31} or time to amplitude converters^{24,25}. However, we note that typically the *experimental resolution* for switching current measurements is not limited by the instrumental resolution of the data acquisition hardware but rather by the residual current and voltage noise in the junction bias electronics. Thus the most important aspect in a well designed measurement setup is the reduction of the external interference by the use of appropriate filtering techniques together with low noise analog electronics.

VI. DATA ANALYSIS

A. Thermal Activation

At temperatures $T > T^*$ the escape of the phase is dominated by thermal activation. At a fixed bias current the activation rate is given by Eq. (7). Using Eq. (11), the experimental escape rate $\Gamma(I)$ is determined from the $P(I)$ data and compared with the predictions of Eq. (7).

To perform this comparison we rewrite Eq. (7) using

the known bias current dependences of the approximated barrier height (6) and the small amplitude oscillation frequency (5) in the following form

$$\left(\ln \frac{2\pi\Gamma(I)}{a_t\omega_0^\phi(I)} \right)^{2/3} = \left(\frac{E_J}{k_B T_{\text{esc}}} \frac{4\sqrt{2}}{3} \right)^{2/3} \frac{1}{I_c} (I_c - I), \quad (12)$$

where we have introduced the effective escape temperature T_{esc} ¹³. The left hand side of Eq. (12) is then calculated in a first iteration using the experimental data $\Gamma(I)$ and $a_t\omega_0^\phi(I)$ estimated approximating the initially unknown value of I_c by the maximum measured switching current I_{max} and using $C = 1.61 \text{ pF}$ determined from independent microwave resonance activation measurements on the same sample³⁸. Because the right hand side of Eq. (12) is a linear function of the bias current I , both the critical current I_c in absence of fluctuations and the effective temperature T_{esc} of the thermal activation process can be determined from a linear fit of the experimental data to the right hand side of Eq. (12). Accordingly, we find

$$I_c = \frac{c_{\text{const}}}{c_{\text{lin}}}, \quad (13)$$

$$T_{\text{esc}} = \frac{1}{k_B} \frac{\Phi_0}{2\pi} \frac{4\sqrt{2}}{3} \frac{1}{c_{\text{const}}^{1/2} c_{\text{lin}}}, \quad (14)$$

where c_{const} and c_{lin} are the two fitting parameters. The values of I_c and T_{esc} are then found with high accuracy by iteratively repeating the fitting procedure with the value of I_c found in the previous iteration¹⁰. This procedure is converging quickly due to the logarithmic dependence of the left hand side of Eq. (12) on I_c .

1. The thermal prefactor in the extremely low damping limit

We have extracted the effective escape temperature T_{esc} from the experimental data according to the procedure described above taking into account the thermal prefactor a_t . In the simple transition state theory, the thermal prefactor is unity and the escape rate is only determined by the fraction of particles with energy larger than the barrier height. In the high as well as in the low damping regimes the prefactor deviates substantially from unity³⁹.

The exact form of the prefactor is found from a analysis of a classical Langevin equation for the motion of the particle according to Eq. (2) in the presence of fluctuations (see e.g. Refs. 2,39). In the moderate to strong damping limit the value of a_t depends predominantly on the damping and the small oscillation frequency in the junction. In the very strong damping limit, the inertia of the particle can be neglected and its motion becomes diffusive^{7,8}. In the low to extremely low damping regime, however, the distribution of the particles in the well deviates from thermal equilibrium. The thermal escape across the barrier depletes the population within a range of $k_B T$ to the top of the barrier. Therefore, a_t becomes dependent on the barrier height and on temperature. For simplicity, we use an approximate analytical expression for the thermal prefactor in the extremely low to low damping regime, relevant for the experimental data presented here, as calculated in Ref. 40

$$a_t = \frac{4a_0}{\left(\sqrt{1 + \frac{a_0 Q k_B T}{1.8 U_0^\phi}} + 1\right)^2}, \quad (15)$$

where a_0 is a numerical constant close to unity. An exact calculation of a_t valid in all damping regimes can be found in Ref. 2.

In a first step, T_{esc} has been evaluated for $a_t = 1$. Under this assumption the escape temperatures extracted from the data deviates more than 100 mK from the bath temperature at $T > T^*$, see open symbols in Fig. 5. The difference $T_{\text{esc}} - T$ even increases with increasing temperature, as shown in the inset of Fig. 5. This deviation is too large to be due to an inaccurate estimate of the junction capacitance or errors in the calibration of the current measurement, thus, indicating the importance of the thermal prefactor.

In a second step, we used the thermal prefactor given by the expression (15) in the calculation of the left hand side of Eq. (12) in our data analysis scheme. We used the junction resistance R as the adjustable parameter determining the junction quality factor Q . We found good agreement between the extracted T_{esc} and the bath temperature T for $R = 500 \Omega$ neglecting its temperature dependence, see solid symbols in Fig. 5. With the low damping prefactor (15), the difference $|T_{\text{esc}} - T|$ is less than 75 mK in the temperature range above T^* , as shown by the solid symbols in the inset of Fig. 5. The

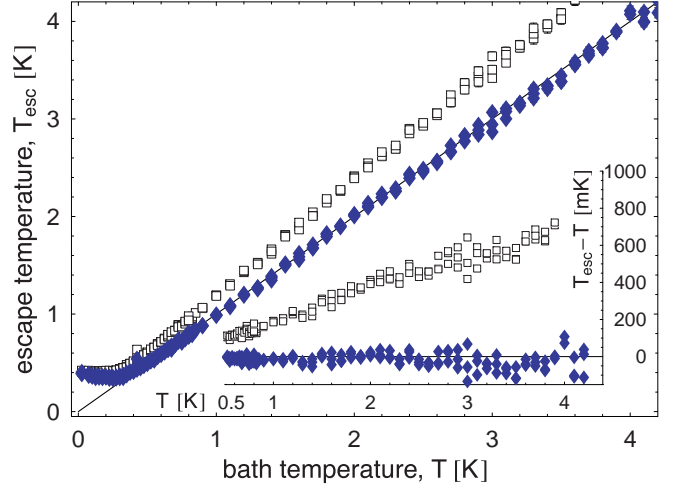


FIG. 5: Escape temperature T_{esc} extracted from experimental data versus bath temperature T for $a_t = 1$ (open symbols) and a_t according to Eq. (15) (solid symbols). At high T the statistical error in T_{esc} extracted from the fitting procedure is approximately given by the symbol size, at low T it is substantially less than the symbol size. The solid line corresponds to $T = T_{\text{esc}}$. The inset shows $T_{\text{esc}} - T$.

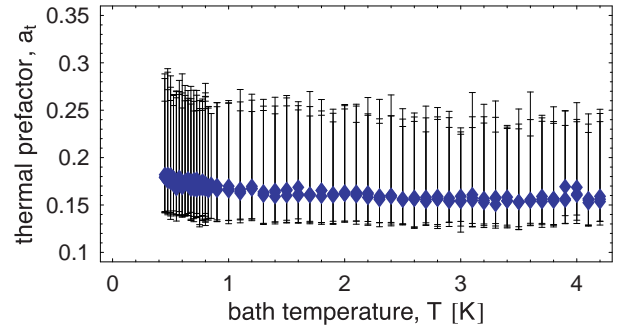


FIG. 6: Thermal prefactor a_t [Eq. (15)] calculated at the most probable switching current I_p versus bath temperature T . The error bars indicate the value of a_t at the minimum I_{min} and maximum switching current I_{max} within each $P(I)$ distribution.

effective resistance used for the fit is in good agreement with the sub-gap resistance determined from the dc current voltage characteristic of the junction.

In Fig. 6, the thermal prefactor a_t evaluated at the most probable switching current I_p is plotted versus temperature for $T > T^*$. Independently of the bath temperature, the mean value of a_t is approximately 0.17. This weak temperature dependence can be attributed to the almost constant ratio of $k_B T / U_0^\phi(I_p)$ for the switching data measured at different temperatures, see Eq. (15). At a fixed bath temperature, the bias current variation within a single $P(I)$ distribution results in a noticeable variation of a_t . The value of a_t at the minimum and maximum switching currents I_{min} and I_{max} is indicated in Fig. 6 by error bars.

Thus, the experimental data is explained with good accuracy by the classical model of the thermal activation of the phase over a potential barrier in the presence of extremely small damping. The quality factor used for the extraction of the effective escape temperature is in agreement with the value determined from the sub gap resistance of the junction.

2. Thermal activation in the presence of energy levels

In thermal activation theory, it is assumed that the particle energies in the well are continuously distributed. For the sample considered here, however, the quantization of the energy of the small amplitude oscillations of the phase may be relevant. In fact, we found direct evidence for the energy level quantization of the phase in this sample by using microwave spectroscopy³⁸.

To address this issue we calculate the approximate number of levels in the well at a given bias current as

$$n_{\max} = \frac{U_0^\phi}{\hbar\omega_0^\phi}, \quad (16)$$

neglecting the anharmonicity of the well. Eq. (16) has been evaluated at the most probable switching current I_p at each temperature, see Fig. 7a. In the quantum tunneling regime at $T < T^*$, we find that there are only a few levels in the well ($n_{\max} \leq 3$). The number of levels in the well at the relevant switching currents increases approximately linearly with temperature from about 5 levels at 1 K to about 20 levels at 4 K. Additionally we have evaluated the level separation $\Delta E = \hbar\omega_0^\phi(I)$ in harmonic approximation at the most probable switching current I_p , see Fig. 7b. At temperatures below 1 K the level separation is much larger than $k_B T$ and at temperatures above 1 K it is comparable with $k_B T$. These facts indicate that the energy level structure may be relevant for the process of the escape of the phase even at temperatures $T > T^*$.

To analyze the effect of the level quantization on the escape of the phase at high temperatures we have made use of the Larkin Ovchinnikov theory³². In the framework of their model the escape of the phase is considered in terms of tunneling out of the well from individual energy levels. The overall escape rate $\Gamma_{LO}(I)$ depends on the population of different levels, which is determined by the coupling to the thermal bath. To apply the Larkin Ovchinnikov theory, we have calculated the energy level structure of the phase in the potential in dependence on the bias current I . The matrix elements for transitions between individual levels have been evaluated and the resulting escape rate has been calculated by solving a master equation for the dynamics of the system. From the escape rate $\Gamma_{LO}(I)$ we have calculated $P(I)$ distributions in a wide temperature range.

The calculated $P(I)$ distributions at temperatures well below T^* , when essentially only the ground state is populated, were in good agreement with the distributions calculated using the WKB approximation for the tunneling

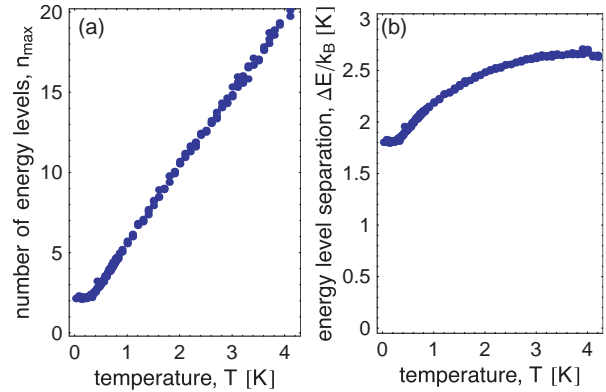


FIG. 7: a) Approximate number of quantized energy levels n_{\max} in the well at the most probable switching current I_p versus the bath temperature T . b) Harmonic approximation of energy level separation $\Delta E/k_B$ at I_p in Kelvin versus T .

from the ground state. At temperatures above T^* , the width of the distribution calculated using Larkin Ovchinnikov theory increased with temperature as expected. We have evaluated these calculated data in the same way as the experimental data, see Sec VIA 1. We found that the calculated histograms are consistent with the classical prediction for a low damping thermal prefactor. Thus in the high temperature limit the results of the Larkin Ovchinnikov theory are in agreement with the predictions of purely classical thermal activation theory. More details on this analysis will be presented elsewhere⁴¹.

B. Quantum Tunneling

At temperatures below the crossover temperature²⁸

$$T^* = \frac{\hbar\omega_0^\phi}{2\pi k_B} \left[\left(1 + \left(\frac{1}{2Q} \right)^2 \right)^{1/2} - \frac{1}{2Q} \right] \quad (17)$$

the escape of the phase from the potential well is dominated by quantum tunneling through the barrier. According to Eq. (17), the crossover temperature T^* for this sample at the most probable switching current I_p is predicted to be approximately 282 mK, which is in good agreement with our experimental findings, see Fig. 4. Since the quality factor of this sample is bounded by $Q > 100$, the reduction of T^* in comparison to the ideal case of $Q = \infty$ is less than one percent. Accordingly, the reduction of the tunneling rate due to dissipation is small.

Furthermore, we have compared the measured $P(I)$ distributions for $T \ll T^*$ to the predicted distributions calculated using the quantum tunneling rate (8). As an example, the data for $T = 25$ mK are shown in Fig. 8 by solid symbols. The quantum tunneling distribution $P_q(I)$ calculated for $I_c = 325.05 \mu\text{A}$ and $C = 1.61 \text{ pF}$

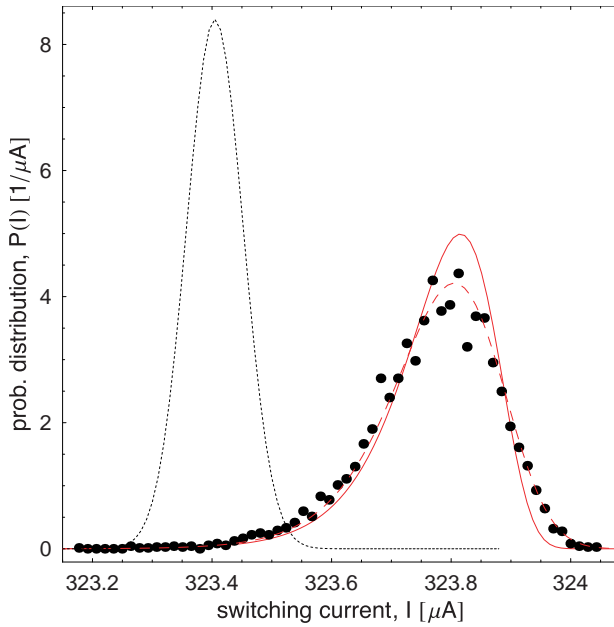


FIG. 8: Measured switching current distribution $P(I)$ at $T = 25\text{mK}$ (solid symbols). The solid line is the predicted switching current distribution $P_q(I)$ in the quantum tunneling regime for $I_c = 325.05 \mu\text{A}$ and $C = 1.61 \text{ pF}$. The $P_q(I)$ distribution broadened by residual experimental noise modeled by gaussian distribution with $\sigma_I = 47.5 \text{ nA}$ (dotted line) is shown by the dashed line.

is shown by the solid line. The critical current I_c was extracted from fits to the data in the thermal regime. As it has been already said above, the capacitance C was determined with high accuracy in independent spectroscopic measurements of the energy level structure of the same sample³⁸. The most probable switching current of the calculated distribution is in good agreement with experimental data. However, the width of the measured distribution is slightly bigger than the predicted one, which is most likely due to the finite residual electromagnetic interference in the measurement setup. To quantify this effect, we have calculated the convolution of the predicted quantum tunneling distribution $P_q(I)$ with a gaussian current distribution with a standard deviation of $\sigma_I = 47.5 \text{ nA}$, shown by the dotted line centered about $I = 323.4 \mu\text{A}$. The resulting distribution, shown by the dashed line in Fig. 8, accurately fits to the experimental data.

VII. CONCLUSIONS

We have developed an experimental setup for the investigation of the escape of the phase in a current-biased

Josephson tunnel junction. Using a timing technique we are able to achieve a high instrumental resolution in the switching current measurement of a Josephson junction. The relative resolution of the switching current measurements demonstrated in this paper is better than 3.7×10^{-4} . This distribution width σ_I/I_c is comparable to the highest resolution measurements of this type performed so far. Using the described technique we have investigated the escape of phase in a high-quality $5 \times 5 \mu\text{m}^2$ Nb-Al/AlO_x-Nb tunnel junction with a relatively large critical current of $I_c \approx 325 \mu\text{A}$. At temperatures above the crossover temperature of $T^* \approx 300 \text{ mK}$ the escape is dominated by thermal activation. Due to the high quality factor of the junction ($Q > 100$) the thermal activation is observed in the limit of extremely low damping. The thermal prefactor a_t extracted from the experimental data is varying between 0.1 to 0.3 depending on bias current and temperature. At temperatures below T^* , the value of which agrees well with the theoretical predictions, the escape of the phase by quantum mechanical tunneling is observed. Due to the high Q -factor of the junction, the tunneling rate is only weakly suppressed by dissipation.

Recent developments in the field of quantum information processing have strongly increased the interest in research on the quantum properties of Josephson junction systems^{21,22,23}. Using the measurement technique and setup described in this paper the quantum mechanical properties of current biased Josephson junctions can be investigated with high accuracy. In particular, we are currently applying this technique for the experimental investigation of the theoretically predicted^{42,43} but not yet observed quantum properties of a single vortex in a long Josephson junction⁴⁴.

Acknowledgments

We would like to thank A. Kemp, S. Lebeda, G. Logvenov, K. Urlich and M. Schuster for their technical help. We are indebted to M. H. Devoret, M. Fistul and V. Kurin for useful discussions and to C. van der Wal, R. Schouten for sharing their experience in low temperature transport measurements with us. We acknowledge the partial financial support of this project by the Deutsche Forschungsgemeinschaft (DFG) and by D-Wave Systems Inc..

* wallraff@physik.uni-erlangen.de

† Scientific Centre of Physical Technologies, National

- Academy of Sciences, 61145 Kharkov, Ukraine
- [‡] Previous address: D-Wave Systems Inc. 1985 West Broadway Vancouver, BC V6J 4Y3, Canada; Current address: Department of Microelectronics and Nanoscience, MC2, Chalmers University of Technology and Göteborg University, S-412 96 Gothenburg, Sweden
- ¹ H. A. Kramers, *Physica* **7**, 284 (1940).
 - ² P. Hänggi, P. Talkner, and M. Borkovec, *Rev. Mod. Phys.* **62**, 251 (1990).
 - ³ A. O. Caldeira and A. J. Leggett, *Phys. Rev. Lett.* **46**, 211 (1981).
 - ⁴ M. H. Devoret, D. Esteve, C. Urbina, J. Martinis, A. Cleland, and J. Clarke, in *Quantum tunneling in condensed media* (North-Holland, 1992).
 - ⁵ W. C. Stewart, *Appl. Phys. Lett.* **12**, 277 (1968).
 - ⁶ D. E. McCumber, *J. Appl. Phys.* **39**, 3113 (1968).
 - ⁷ D. Vion, M. Götz, P. Joyez, D. Esteve, and M. Devoret, *Phys. Rev. Lett.* **77**, 3435 (1996).
 - ⁸ J. M. Martinis and R. L. Kautz, *Phys. Rev. Lett.* **63**, 1507 (1989).
 - ⁹ T. Fulton and L. Dunkelberger, *Phys. Rev. B* **9**, 4760 (1974).
 - ¹⁰ M. Castellano, R. Leoni, G. Torrioli, F. Chiarello, C. Cosmelli, A. Costantini, G. Diambrini-Palazzi, P. Carelli, R. Cristiano, and L. Frunzio, *J. Appl. Phys.* **80**, 2922 (1996).
 - ¹¹ B. Ruggiero, C. Granata, V. G. Palmieri, A. Esposito, M. Russo, and P. Silvestrini, *Phys. Rev. B* **57**, 134 (1998).
 - ¹² J. M. Martinis, M. H. Devoret, and J. Clarke, *Phys. Rev. B* **35**, 4682 (1987).
 - ¹³ M. H. Devoret, J. M. Martinis, and J. Clarke, *Phys. Rev. Lett.* **55**, 1908 (1985).
 - ¹⁴ R. F. Voss and R. A. Webb, *Phys. Rev. Lett.* **47**, 265 (1981).
 - ¹⁵ L. D. Jackel, J. P. Gordon, E. L. Hu, R. E. Howard, L. A. Fetter, D. M. Tennant, R. W. Eprorth, and J. Kurkijärvi, *Phys. Rev. Lett.* **47**, 697 (1981).
 - ¹⁶ P. Silvestrini, V. G. Palmieri, B. Ruggiero, and M. Russo, *Phys. Rev. Lett.* **79**, 3046 (1997).
 - ¹⁷ S. Han, Y. Yu, X. Chu, C. S., and Z. Wang, *Science* **283**, 1457 (2001).
 - ¹⁸ J. E. Mooij, T. P. Orlando, L. Levitov, L. Tian, C. H. van der Wal, and S. Lloyd, *Science* **285**, 1036 (1999).
 - ¹⁹ L. B. Ioffe, V. B. Geshkenbein, M. V. Feigel'man, A. L. Fauchere, and G. Blatter, *Nature* **398**, 679 (1999).
 - ²⁰ M. F. Bocko, A. M. Herr, and M. J. Feldman, *IEEE Trans. Appl. Supercond.* **7**, 3638 (1997).
 - ²¹ Y. Nakamura, Y. A. Pashkin, and J. S. Tsai, *Nature* **398**, 786 (1999).
 - ²² J. R. Friedman, V. Patel, W. Chen, S. K. Tolpygo, and J. E. Lukens, *Nature* **406**, 43 (2000).
 - ²³ C. H. van der Wal, A. C. J. ter Haar, F. K. Wilhelm, R. N. Schouten, C. J. P. M. Harmans, T. P. Orlando, S. Lloyd, and J. E. Mooij, *Science* **290**, 773 (2000).
 - ²⁴ P. Silvestrini, S. Pagano, R. Cristiano, O. Liengme, and K. E. Gray, *Phys. Rev. Lett.* **60**, 844 (1988).
 - ²⁵ P. Silvestrini, O. Liengme, and K. E. Gray, *Phys. Rev. B* **37**, 1525 (1988).
 - ²⁶ E. Turlot, D. Esteve, C. Urbina, J. M. Martinis, M. H. Devoret, S. Linkwitz, and H. Grabert, *Phys. Rev. Lett.* **62**, 1788 (1989).
 - ²⁷ S. Washburn, R. A. Webb, R. F. Voss, and S. M. Faris, *Phys. Rev. Lett.* **54**, 2712 (1984).
 - ²⁸ H. Grabert and U. Weiss, *Phys. Rev. Lett.* **53**, 1787 (1984).
 - ²⁹ A. O. Caldeira, *Ann. of Phys.* **149**, 374 (1983).
 - ³⁰ A. J. Leggett, in *Percolation, localization, and superconductivity* (Plenum Press, New York, 1984).
 - ³¹ B. Ruggiero, M. G. Castellano, G. Torrioli, C. Cosmelli, F. Chiarello, and V. G. Palmieri, *Phys. Rev. B* **59**, 177 (1999).
 - ³² A. I. Larkin and Y. N. Ovchinnikov, *Sov. Phys. JETP* **64**, 185 (1986).
 - ³³ K. S. Chow, D. A. Brown, and V. Ambegaokar, *Phys. Rev. B* **37**, 1624 (1988).
 - ³⁴ P. Kopietz and S. Chakravarty, *Phys. Rev. B* **38**, 97 (1988).
 - ³⁵ M. H. Devoret, J. M. Martinis, D. Esteve, and J. Clarke, *Phys. Rev. Lett.* **53**, 1260 (1984).
 - ³⁶ A. B. Zorin, *Rev. Sci. Instrum.* **66**, 4296 (1995).
 - ³⁷ D. Vion, P. F. Orfila, P. Joyez, D. Esteve, and M. H. Devoret, *J. Appl. Phys.* **77**, 2519 (1995).
 - ³⁸ A. Wallraff, T. Duty, A. Lukashenko, C. Coqui, and A. V. Ustinov, (unpublished).
 - ³⁹ U. Weiss, *Quantum dissipative systems* (World Scientific, 1999), 2nd ed.
 - ⁴⁰ M. Büttiker, E. P. Harris, and R. Landauer, *Phys. Rev. B* **28**, 1268 (1983).
 - ⁴¹ T. Duty and A. Wallraff, (unpublished).
 - ⁴² T. Kato and M. Imada, *J. Phys. Soc. Jpn.* **65**, 2963 (1996).
 - ⁴³ A. Shnirman, E. Ben-Jacob, and B. A. Malomed, *Phys. Rev. B* **56**, 14677 (1997).
 - ⁴⁴ A. Wallraff, *Fluxon Dynamics in annular Josephson junctions: From relativistic strings to quantum particles* (Verlag Lehrstuhl für Mikrocharakterisierung, 2000), ISBN 3-932392-29-9.
 - ⁴⁵ Thermocoax GmbH, Hamburg, Germany
 - ⁴⁶ Stanford Research Instruments, Model SR 620 Universal Time Interval Counter